Switching classical and quantum nonreciprocities with a single spinning resonator

Yonglin Xiang,[1,*] Yunlan Zuo,[1,*] Xun-Wei Xu,[1] Ran Huang,[2,†] and Hui Jing[1,3,‡]

[1]*Key Laboratory of Low-Dimensional Quantum Structures and Quantum Control of Ministry of Education, Department of Physics and Synergetic Innovation Center for Quantum Effects and Applications, Hunan Normal University, Changsha 410081, China*

[2]*Theoretical Quantum Physics Laboratory, RIKEN Cluster for Pioneering Research, Wako-shi, Saitama 351-0198, Japan*

[3]*Synergetic Innovation Academy for Quantum Science and Technology, Zhengzhou University of Light Industry, Zhengzhou 450002, China*

(Received 14 February 2023; revised 22 August 2023; accepted 18 September 2023; published 4 October 2023)

We study how to achieve, manipulate, and switch classical or quantum nonreciprocal effects of light with a spinning Kerr resonator. In particular, we show that even when there is no classical nonreciprocity (i.e., with the same mean number of photons for both clockwise and counterclockwise propagating modes), it is still possible to realize nonreciprocity of quantum correlations of photons in such a device. Also, by tuning the angular velocity and the optical backscattering strength, purely higher-order quantum nonreciprocity can appear, featuring qualitatively different third-order optical correlations, even in the absence of any nonreciprocity for both the mean photon number and its second-order correlations. The possibility to switch a single device between a classical isolator and a purely quantum directional system can provide more functions for nonreciprocal materials and new opportunities to realize novel quantum effects and applications, such as nonreciprocal multiphoton blockade, one-way photon bundles, and back-action-immune quantum communications.

DOI: 10.1103/PhysRevA.108.043702

I. INTRODUCTION

Optical nonreciprocity, featuring different responses of light when the input and output ports are interchanged, plays a key role in fundamental studies and applications of modern optics, such as directional laser engineering, invisible sensing, and back-action-immune optical communications [1]. In recent years, without using any bulky magnetic materials [2,3], various ways have been demonstrated to create optical on-chip nonreciprocity, such as spatiotemporal modulation [4–11], optical nonlinearities [12–31], non-Hermitian structures [32–35], quantum squeezing [36], and controllable motion of atoms or solid devices [37–61]. Particularly, by spinning a single device, it is possible to achieve nonreciprocal transmissions of light, sound, or a thermal field, without relying on any nonlinear medium [62–64], providing flexible new ways to achieve nanoparticle sensing [65–67], optical gyroscopes [68], and quantum or topological directional control [69–73]. Also, by further integrating with existing techniques of quantum nonlinear optics, purely quantum nonreciprocal effects can be achieved in such spinning systems, such as nonreciprocal photon blockade [46–50] and nonreciprocal quantum entanglement [51–54]. We note that, in a very recent experiment, quantum nonreciprocal correlations of photons were already observed in experiments using cavity atoms or an optical nonlinear system [74,75]. However, until now, in the absence of any classical nonreciprocity, the possibility of achieving one-way control of higher-order quantum correlations has not been studied.

Here, in this work, we show how to achieve coherent switch of classical and quantum nonreciprocities of photons and how to realize a class of higher-order quantum nonreciprocity with a single spinning resonator. We find that, by tuning both the angular speed of the resonator and the optical backscattering strength, one can switch the functions of the device between a classical isolator and a purely quantum directional system. Also, a particular type of higher-order quantum nonreciprocity can emerge where both of the mean photon numbers and the second-order correlations are reciprocal, but the third-order correlation function is nonreciprocal. We refer to this phenomenon as purely higher-order quantum nonreciprocity (PH-QNR). Particularly, we note that the backscattering due to material imperfections can induce the PH-QNR, in comparison with that in ideal devices. Our findings indicate a promising way to achieve novel nonreciprocal effects, which is useful in realizing chiral quantum networks [76–79] and invisible sensing [80,81].

The remainder of this paper is organized as follows. In Sec. II, we introduce the physical system of a spinning Kerr resonator with a tapered fiber. In Sec. III, we study the quantum and classical nonreciprocities in the ideal spinning resonator. In Sec. IV, we explore the quantum and classical nonreciprocities for systems with backscattering. In particular, we reveal a purely higher-order quantum nonreciprocity. In Sec. V, we give a summary.

II. PHYSICAL SYSTEM

As shown in Fig. 1(a), we consider a spinning Kerr resonator evanescently coupled with a tapered fiber, and each

*These authors contributed equally to this work.
†ran.huang@riken.jp
‡jinghui73@foxmail.com

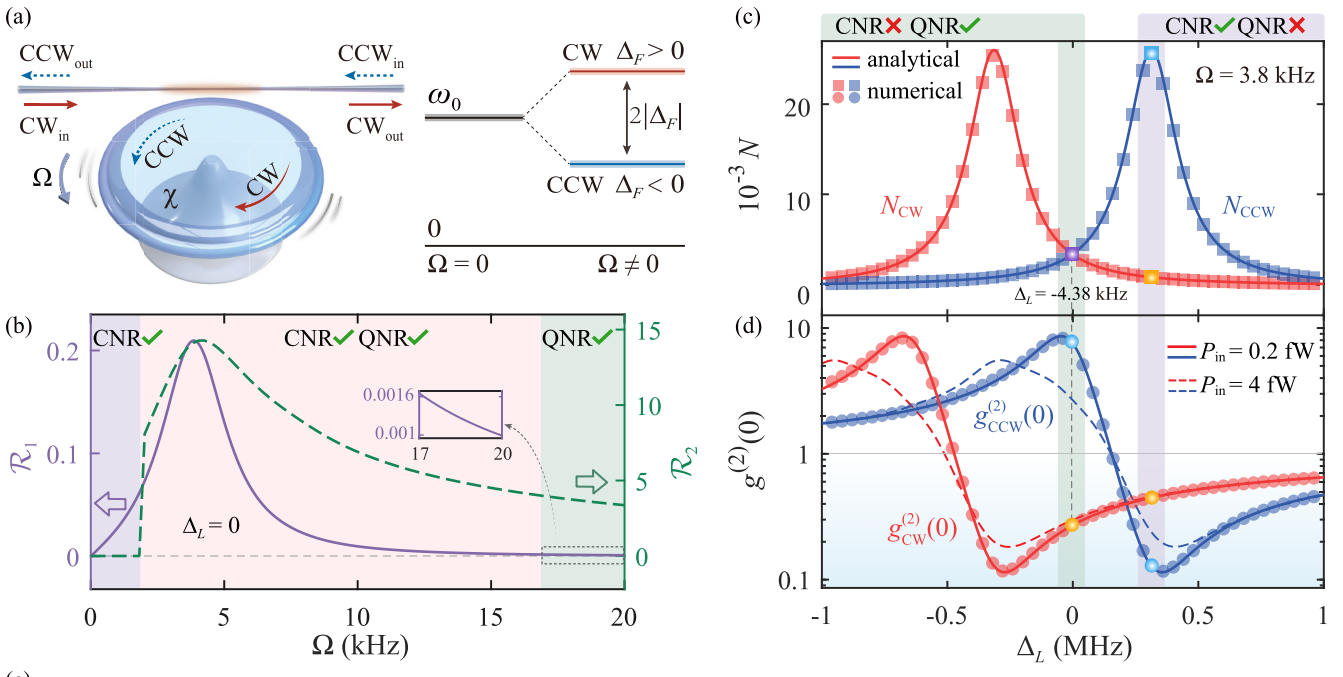

(e)

Dimensionless parameters (γ, cavity loss rate)	Values
Kerr parameter χ/γ	1.3
Driving amplitude ξ/γ	0.08
Angular velocity Ω/γ	0 – 0.08

CNR ✓	$N_{\rm CW} \neq N_{\rm CCW}$
QNR ✓	$g^{(2)}_{\rm CW}(0) < 1,\ g^{(2)}_{\rm CCW}(0) > 1;$ $g^{(2)}_{\rm CW}(0) > 1,\ g^{(2)}_{\rm CCW}(0) < 1$

FIG. 1. Quantum and classical nonreciprocities. (a) The whispering-gallery-mode resonator with Kerr-type nonlinearity χ spinning at an angular velocity Ω. By fixing the CCW rotation of the resonator, $\Delta_F > 0$ ($\Delta_F < 0$) corresponds to the situation of driving the CW (CCW) mode. (b) The classical (quantum) nonreciprocity ratio $\mathcal{R}_1$ ($\mathcal{R}_2$) versus the angular velocity Ω for $\Delta_L = 0$, where the solid and dashed curves indicate $\mathcal{R}_1$ and $\mathcal{R}_2$, respectively. The inset shows that $\mathcal{R}_1 \sim 0.0016$ when $\Omega = 17\,\text{kHz}$ (i.e., $\Omega/\gamma = 0.07$). By further increasing Ω, $\mathcal{R}_1$ gradually approaches 0. (c) The mean photon number N and (d) the second-order correlation function $g^{(2)}(0)$ versus the optical detuning Δ_L for different input directions at $\Omega = 3.8\,\text{kHz}$ (i.e., $\Omega/\gamma = 0.016$). The solid curves and markers (squares, circles) are analytical and numerical solutions at $P_{\rm in} = 0.2\,\text{fW}$ (i.e., $\xi/\gamma = 0.08$), respectively. When we take the parameter $P_{\rm in} = 4\,\text{fW}$ (i.e., $\xi/\gamma = 0.36$) in the experiment [82] (dashed curves), the quantum nonreciprocal feature can still be achieved. (e) The values and definitions of the main dimensionless parameters that we used in our calculations. The other parameters are given in the main text.

side of the fiber serves as both an input port and an output port. Depending on the input port, light is coupled to circulate in the resonator in either the clockwise (CW) or counterclockwise (CCW) direction. Recently, 99.6% optical isolation was realized experimentally by using a spinning resonator [44]. In this experiment, the resonator is mounted on a turbine and rotated along its axis. The tapered fiber is made by heating and pulling a standard single-mode telecommunications fiber, which is stabilized at a height of several nanometers above the rapidly spinning resonator via the "self-adjustment" aerodynamic process. Here, for a resonator spinning along a fixed direction at angular velocity Ω, the resonance frequencies of the CW and CCW modes experience an opposite Sagnac-Fizeau shift, i.e., $\omega_0 \to \omega_0 + \Delta_F$, with [83]

$$\Delta_F = \pm \frac{n_1 r \Omega \omega_0}{c}\left(1 - \frac{1}{n_1^2} - \frac{\lambda}{n_1}\frac{dn_1}{d\lambda}\right), \tag{1}$$

where ω_0 is the optical frequency of the nonspinning resonator, c (λ) is the speed (wavelength) of light in a vacuum, and n_1 and r are the refractive index and radius of the resonator, respectively. The dispersion term $dn_1/d\lambda$, characterizing the relativistic origin of the Sagnac effect, is relatively small in typical materials (up to about 1%) [44,83]. By spinning the resonator along the CCW direction, we have $\Delta_F > 0$ ($\Delta_F < 0$) for the case with the driven the CW (CCW) mode, i.e., $\omega_{\rm cw,ccw} = \omega_0 \pm |\Delta_F|$ [see Fig. 1(a)].

In the frame rotating at the drive frequency ω_L, the Hamiltonian of the system reads ($\hbar = 1$)

$$\hat{H}_1 = (\Delta_L + \Delta_F)\hat{a}^\dagger\hat{a} + \chi\hat{a}^\dagger\hat{a}^\dagger\hat{a}\hat{a} + \xi(\hat{a}^\dagger + \hat{a}), \tag{2}$$

where $\Delta_L = \omega_0 - \omega_L$ is the optical detuning between the driving field and the cavity field, $\hat{a}$ ($\hat{a}^\dagger$) is the optical annihilation (creation) operator, and $\chi = \hbar\omega_0^2 c n_2/(n_0^2 V_{\rm eff})$ is the Kerr parameter, with $n_0(n_2)$ being the linear (nonlinear) refraction index and $V_{\rm eff}$ being the effective mode volume. $\xi = \sqrt{\gamma P_{\rm in}/(\hbar\omega_L)}$ is the driving amplitude with cavity loss rate γ and driving power $P_{\rm in}$.

The energy eigenstates of this system are the Fock states $|n\rangle$ ($n = 0, 1, 2, \ldots$) with eigenenergies

$$E_n = n\Delta_L + n\Delta_F + (n^2 - n)\chi, \tag{3}$$

where n is the cavity photon number. The positive and negative values of Δ_F describe upper and lower shifts of energy levels, respectively [Fig. 1(a)], and the values of $|\Delta_F|$ are

proportional to Ω. For the same input light, due to the opposite frequency shift for the counterpropagating modes, nonreciprocity can appear.

The experimentally accessible parameters we used here are [82,84–88] $\lambda = 1550\,\mathrm{nm}$, $Q = 5 \times 10^9$, $V_{\mathrm{eff}} = 150\,\mu\mathrm{m}^3$, $n_2 = 2 \times 10^{-15}\,\mathrm{m}^2/\mathrm{W}$, $n_0 = 1.4$, $P_{\mathrm{in}} = 0.2\,\mathrm{fW}$, and $r = 30\,\mu\mathrm{m}$. In addition, we set angular velocity $\Omega = 3.8$ and 5.8 kHz, which are experimentally accessible parameters in Ref. [44]. We note that V_{eff} is typically 10^2–$10^4\,\mu\mathrm{m}^3$ [84,85] and Q is typically 10^9–10^{12} [86,87]. The Kerr coefficient can reach $n_2 = 2 \times 10^{-15}\,\mathrm{m}^2/\mathrm{W}$ for materials with potassium titanyl phosphate [88], i.e., $\chi/\gamma = 1.3$. The driving power can reach $P_{\mathrm{in}} = 4\,\mathrm{fW}$ (i.e., $\xi/\gamma = 0.36$) in the experiment [82]. Here, we have chosen the experimentally accessible values $\chi/\gamma = 1.3$ and $\xi/\gamma = 0.08$. Also we have confirmed that even for the values taken in the experiment [82], i.e., $\xi/\gamma = 0.36$, the quantum nonreciprocal feature can still be achieved, as shown in Fig. 1(d) (dashed curves).

III. CLASSICAL AND QUANTUM NONRECIPROCITIES

The classical features of this work can be characterized by the mean photon number N:

$$N = \langle \hat{a}^\dagger \hat{a} \rangle. \tag{4}$$

The condition of classical nonreciprocity (CNR) is

$$N_{\mathrm{CW}} \neq N_{\mathrm{CCW}}. \tag{5}$$

Note that in this work, we use the subscripts CW and CCW to denote the cases with the driven CW and CCW modes, respectively.

The quantum features can be characterized by the quantum correlation function $g^{(2)}(0)$:

$$g^{(2)}(0) = \frac{\langle \hat{a}^{\dagger 2} \hat{a}^2 \rangle}{\langle \hat{a}^\dagger \hat{a} \rangle^2}. \tag{6}$$

The conditions $g^{(2)}(0) < 1$ and $g^{(2)}(0) > 1$ characterize single-photon blockade and photon-induced tunneling [89,90], respectively, which are two distinct quantum effects with different photon-number statistics, i.e., photon antibunching and bunching [91,92]. Thus, we refer to the effect of photon antibunching in one direction and bunching in the other direction as quantum nonreciprocity. Here, the condition of quantum nonreciprocity (QNR) is given by

$$g^{(2)}_{\mathrm{CW}}(0) < 1, \quad g^{(2)}_{\mathrm{CCW}}(0) > 1$$

or

$$g^{(2)}_{\mathrm{CW}}(0) > 1, \quad g^{(2)}_{\mathrm{CCW}}(0) < 1. \tag{7}$$

To better study the classical and quantum nonreciprocities of this system, we define the classical and quantum nonreciprocity ratios as $\mathcal{R}_1$ and $\mathcal{R}_2$, respectively, which are written as

$$\mathcal{R}_1 = 10 \log_{10} \frac{N_{\mathrm{CCW}}}{N_{\mathrm{CW}}}, \quad \mathcal{R}_2 = 10 \log_{10} \frac{g^{(2)}_{\mathrm{CCW}}(0)}{g^{(2)}_{\mathrm{CW}}(0)}. \tag{8}$$

When N_{CW} and N_{CCW} do not satisfy the condition of nonreciprocity in Eq. (5), i.e., classical reciprocity, $\mathcal{R}_1 = 0$. Similarly, when both $g^{(2)}_{\mathrm{CW}}(0)$ and $g^{(2)}_{\mathrm{CCW}}(0)$ are larger or smaller than 1 (i.e., the same quantum effects with identical photon-number statistics occur in both directions), we refer to this effect as quantum reciprocity. Thus, we set $\mathcal{R}_2 = 0$ for this case.

According to the quantum-trajectory method [93], the optical decay can be included in the effective Hamiltonian

$$\hat{H}_{\mathrm{e1}} = \hat{H}_1 - i\frac{\gamma}{2}\hat{a}^\dagger \hat{a}, \tag{9}$$

where $\gamma = \omega_0/Q$ is the cavity loss rate with quality factor Q. Under the weak-driving condition ($\xi \ll \gamma$), the Hilbert space can be truncated to $n = 2$. The state of this system can be expressed as

$$|\varphi(t)\rangle = \sum_{n=0}^{2} C_n(t)|n\rangle, \tag{10}$$

with probability amplitudes C_n. Based on the effective Hamiltonian in Eq. (9) and the wave function in Eq. (10), we can obtain the following equations of motion for the probability amplitudes $C_n(t)$:

$$\begin{aligned}
\dot{C}_0(t) &= -iE_0 C_0(t) - i\xi C_1(t), \\
\dot{C}_1(t) &= -i\Big(E_1 - i\frac{\gamma}{2}\Big)C_1(t) - i\xi C_0(t) - i\xi\sqrt{2}C_2(t), \\
\dot{C}_2(t) &= -i(E_2 - i\gamma)C_2(t) - i\xi\sqrt{2}C_1(t),
\end{aligned} \tag{11}$$

where $E_0 = 0$, $E_1 = \Delta_L + \Delta_F$, and $E_2 = 2(\Delta_L + \Delta_F) + 2\chi$. In the weak-driving case, these probability amplitudes have the following approximation expressions: $C_0 \sim 1$, $C_1 \sim \xi/\gamma$, and $C_2 \sim \xi^2/\gamma^2$. According to the perturbation method [94] for solving the above equations, we can obtain the following probability amplitudes:

$$\begin{aligned}
\dot{C}_0(t) &= -iE_0 C_0(t), \\
\dot{C}_1(t) &= -i\Big(E_1 - i\frac{\gamma}{2}\Big)C_1(t) - i\xi C_0(t), \\
\dot{C}_2(t) &= -i(E_2 - i\gamma)C_2(t) - i\xi\sqrt{2}C_1(t).
\end{aligned} \tag{12}$$

In an initially empty cavity, the initial conditions can be set as

$$\begin{aligned}
C_0(0) &= C_0(0), \\
C_1(0) &= C_2(0) = 0.
\end{aligned} \tag{13}$$

Therefore, we can obtain the solution of the zero-photon amplitude:

$$C_0(t) = C_0(0)\exp(-iE_0 t). \tag{14}$$

We introduce the slow-varying amplitudes to solve this equation:

$$\begin{aligned}
C_1(t) &= c_1(t)\exp\Big[-i\Big(E_1 - i\frac{\gamma}{2}\Big)t\Big], \quad C_1(0) = c_1(0), \\
C_2(t) &= c_2(t)\exp[-i(E_2 - i\gamma)t], \quad C_2(0) = c_2(0).
\end{aligned} \tag{15}$$

Then, based on the solution of the zero-photon amplitude in Eq. (14) and the above equations, we can obtain the solutions

of the equations of motion for the probability amplitudes,

$$\begin{aligned} C_0(t) &= C_0(0)\mathcal{A}_0, \\ C_1(t) &= -\xi C_0(0)(\mathcal{A}_0 - \mathcal{A}_1)/\Big(E_1 - i\frac{\gamma}{2}\Big), \\ C_2(t) &= \sqrt{2}\xi^2 C_0(0)(\mathcal{B}_0 - \mathcal{B}_1)/\Big(E_1 - i\frac{\gamma}{2}\Big), \end{aligned} \tag{16}$$

where

$$\begin{aligned} \mathcal{A}_0 &= \exp(-iE_0 t), \\ \mathcal{A}_1 &= \exp[-i(E_1 - i\gamma/2)t], \\ \mathcal{A}_2 &= \exp[-i(E_2 - i\gamma)t], \\ \mathcal{B}_0 &= (\mathcal{A}_0 - \mathcal{A}_2)/(E_2 - E_0 - i\gamma), \\ \mathcal{B}_1 &= (\mathcal{A}_1 - \mathcal{A}_2)/(E_2 - E_1 - i\gamma/2), \end{aligned} \tag{17}$$

and for the infinite-time limit, we have $\exp(-At) \to 0$ ($t \to \infty$); then the solutions should be

$$\begin{aligned} C_0 &\equiv C_0(\infty) = 1, \\ C_1 &\equiv C_1(\infty) = \frac{-\xi}{(E_1 - i\gamma/2)}, \\ C_2 &\equiv C_2(\infty) = \frac{-\sqrt{2}\xi C_1}{(E_2 - i\gamma)}. \end{aligned} \tag{18}$$

According to the normalized coefficient of the state

$$\mathcal{M} = 1 + |C_1|^2 + |C_2|^2, \tag{19}$$

we can get the probabilities of finding n photons in the resonator as

$$P_n = \frac{|C_n|^2}{\mathcal{M}}. \tag{20}$$

The mean photon number is denoted by N and can be obtained from the above probability distribution as

$$N = \langle \hat{a}^\dagger \hat{a} \rangle = \sum_{n=0}^{2} n P_n. \tag{21}$$

For $\Delta_L = 0$, the mean photon number becomes

$$N = \frac{\xi^4}{\chi\gamma^2\Delta_F + 4\chi\Delta_F^3 + 2\big(\Delta_F^2 + \chi^2 + \gamma^2/4\big)\big(\Delta_F^2 + \gamma^2/4\big)} + \frac{\xi^2}{\Delta_F^2 + \gamma^2/4}. \tag{22}$$

The origin of classical nonreciprocity can be understood from the terms of the Sagnac-Fizeau shift ($\propto \Delta_F$) and its cubic terms ($\propto \Delta_F^3$).

The equal-time (namely, zero-time-delay) second-order correlation function is written as

$$g^{(2)}(0) = \frac{\langle \hat{a}^{\dagger 2}\hat{a}^2 \rangle}{\langle \hat{a}^\dagger \hat{a} \rangle^2} \simeq \frac{(\Delta_L + \Delta_F)^2 + \gamma^2/4}{(\Delta_L + \Delta_F + \chi)^2 + \gamma^2/4}. \tag{23}$$

For $\Delta_L = 0$, photon antibunching [$g^{(2)}(0) < 1$] and bunching [$g^{(2)}(0) > 1$] occur under the conditions of $\Delta_F > -\chi/2$ and $\Delta_F < -\chi/2$, respectively. Therefore, the condition of quantum nonreciprocity, $\mathcal{R}_2 \neq 0$, is given by

$$\Omega > \frac{\chi}{2\alpha}, \quad \alpha = \frac{n_1 r\omega_0}{c}\left(1 - \frac{1}{n_1^2} - \frac{\lambda}{n_1}\frac{dn_1}{d\lambda}\right). \tag{24}$$

This result is in agreement with the results of Fig. 1(b); that is, the transition between quantum reciprocity and nonreciprocity occurs at $\Omega \approx 1.93$ kHz.

To obtain more exact results, we numerically study the full quantum dynamics of the system by solving the master equation [95,96]

$$\dot{\hat{\rho}} = \frac{i}{\hbar}[\hat{\rho}, \hat{H}_1] + \frac{\gamma}{2}(2\hat{a}\hat{\rho}\hat{a}^\dagger - \hat{a}^\dagger\hat{a}\hat{\rho} - \hat{\rho}\hat{a}^\dagger\hat{a}), \tag{25}$$

where $\hat{\rho}$ is the normalized density matrix of the system. The photon-number probability is $P_n = \langle n|\hat{\rho}_{\rm ss}|n\rangle$, with $\hat{\rho}_{\rm ss}$ being the steady-state solutions of the master equation.

Figure 1(b) shows the switching between CNR and QNR when the optical detuning $\Delta_L = 0$. For a nonspinning resonator ($\Omega = 0$), both classical and quantum effects are reciprocal at this point, i.e., $\mathcal{R}_1 = 0$ and $\mathcal{R}_2 = 0$. When the angular velocity Ω is below 1.93 kHz, the classical nonreciprocity appears ($\mathcal{R}_1 > 0$) since the rotation-induced Sagnac effect breaks the degeneracy of the CW and CCW modes, leading to a mode splitting, which makes the light transparent in one direction and opaque in the other, i.e., one-way transmission of the light [44]. At the same time, the quantum nonreciprocity ratio $\mathcal{R}_2$ is always equal to zero, and the quantum effect is reciprocal.

When $\Omega = [1.93\,\text{kHz}, 17\,\text{kHz}]$, the quantum nonreciprocity ($\mathcal{R}_2 > 0$) emerges due to the interplay of both the rotation-induced Sagnac effect and the nonlinearity-induced anharmonicity. The Kerr nonlinearity leads to an anharmonic energy space, which can be further shifted by the Sagnac effect. When the rotation speed is large enough, the energy level of the system satisfies the conditions for photon antibunching in one direction and bunching in the other direction [46].

When Ω exceeds 17 kHz, $\mathcal{R}_1$ gradually approaches zero, but the quantum nonreciprocity still remains ($\mathcal{R}_2 > 0$); this means that quantum nonreciprocity exists even when there is no classical nonreciprocity. We note that quantum nonreciprocity can exist independently of classical nonreciprocity, as shown in a recent experiment [75]. The fundamental reason is that classical and quantum nonreciprocities are two essentially different concepts, which are defined via the mean-photon number and quantum fluctuation. With optical nonlinearity, quantum fluctuations with the same mean-photon number can be different [75]. With such a device, the different nonreciprocities can be tuned by tuning the angular velocity.

In addition, we note that the switching between classical nonreciprocity and pure quantum nonreciprocity can also be achieved by tuning the optical detuning Δ_L [Figs. 1(c) and 1(d)]. As an illustration, for a spinning cavity, by driving the CW (CCW) mode, we have $\Delta_F > 0$ ($\Delta_F < 0$), thus leading to quantum nonreciprocity at $\Delta_L = -4.38$ kHz, i.e., $g^{(2)}_{\rm CW}(0) \sim 0.28$ and $g^{(2)}_{\rm CCW}(0) \sim 7$. At this point, $N_{\rm cw} = N_{\rm ccw}$, the classical effect is reciprocal. When the maximum difference of mean photon numbers from driving the setup from the right and left sides is generated, $N_{\rm CW} \sim 0.001$, and $N_{\rm CCW} \sim 0.0245$. This is a clear signature of classical nonreciprocity. At the same time, we have quantum reciprocity, i.e., $g^{(2)}_{\rm CW}(0) \sim 0.45$ and $g^{(2)}_{\rm CCW}(0) \sim 0.12$.

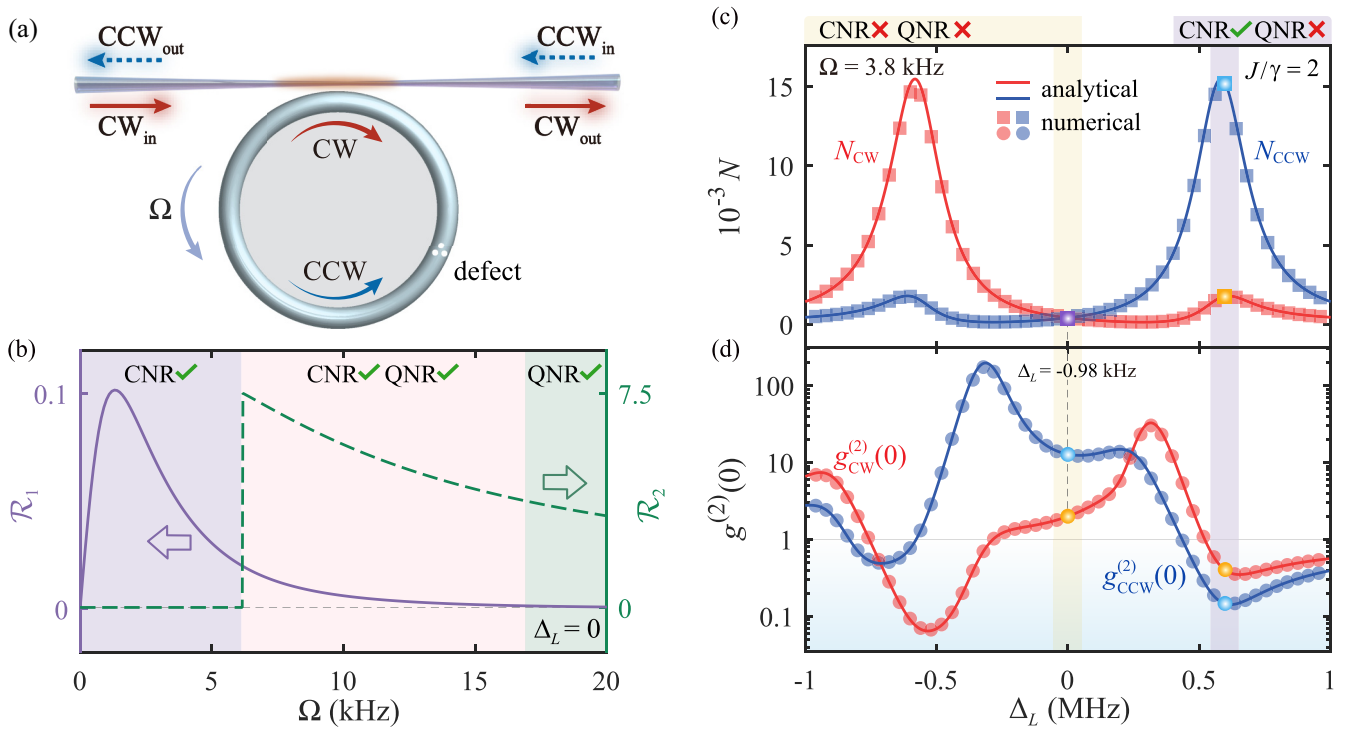

FIG. 2. Quantum and classical nonreciprocities with backscattering. (a) The spinning Kerr resonator with defect-induced backscattering. The CW and CCW modes are coupled via backscattering with strength J. (b) The classical (quantum) nonreciprocity ratio $\mathcal{R}_1$ ($\mathcal{R}_2$) versus the angular velocity Ω for $\Delta_L = 0$, where the solid (dashed) curve indicates $\mathcal{R}_1$ ($\mathcal{R}_2$). (c) The mean photon number N and (d) the second-order correlation function $g^{(2)}(0)$ as a function of Δ_L for different input directions at $\Omega = 3.8$ kHz (i.e., $\Omega/\gamma = 0.016$). The solid curves and markers (squares, circles) are analytical and numerical solutions, respectively. We note that the backscattering rate can reach $J/\gamma = 15$ in the experiment [97], and the mode splitting induced by backscattering is easily experimentally observable for $J/\gamma > 1/2$ [98]. Here, the parameter of the backscattering rate is chosen to be $J/\gamma = 2$; the other parameters are the same as those in Fig. 1.

These results show that a single device switching between a classical isolator and a quantum one-way device can be achieved by adjusting multiple degrees of freedom [51].

IV. QUANTUM AND CLASSICAL NONRECIPROCITIES WITH BACKSCATTERING

Now, we further extend our present study to a more generalized situation. In practice, device imperfections, such as surface roughness and material defect, can cause optical backscattering, as shown in Fig. 2(a). Thus, we discuss the role of backscattering in quantum and classical nonreciprocities. For this aim, we introduce backscattering, as described by the coupling strength J between the CW and CCW modes. The system's Hamiltonian, given in Eq. (2), is transformed to

$$\begin{aligned}\hat{H}_2 =& \sum_{j=1,2}\Delta_j\hat{a}_j^\dagger\hat{a}_j + \sum_{j=1,2}\chi\hat{a}_j^\dagger\hat{a}_j^\dagger\hat{a}_j\hat{a}_j \\ &+ 2\chi\hat{a}_1^\dagger\hat{a}_1\hat{a}_2^\dagger\hat{a}_2 + J\left(\hat{a}_1^\dagger\hat{a}_2 + \hat{a}_2^\dagger\hat{a}_1\right) \\ &+ \xi(\hat{a}_1^\dagger + \hat{a}_1),\end{aligned} \tag{26}$$

where $\hat{a}_1$ ($\hat{a}_1^\dagger$) and $\hat{a}_2$ ($\hat{a}_2^\dagger$) are the annihilation (creation) operators of the CW and CCW modes, respectively. $\Delta_j = \Delta_L \pm |\Delta_F|$ ($j = 1, 2$), and $2\chi\hat{a}_1^\dagger\hat{a}_1\hat{a}_2^\dagger\hat{a}_2$ is the cross-Kerr interaction [14,16,99,100] between the CW and CCW modes.

Optical decay can be included in the effective Hamiltonian [93],

$$\hat{H}_{e2} = \hat{H}_2 - \sum_{j=1,2} i\gamma\hat{a}_j^\dagger\hat{a}_j/2. \tag{27}$$

In the weak-driving case ($\xi \ll \gamma$), the Hilbert space of the system can be restricted to a subspace with few photons. Here, in order to calculate the expressions for the second-order and third-order correlation functions, this Hilbert space is truncated to a subspace with three-photon numbers, i.e., $N = m + n = 3$; the wave function of the system can be expressed as

$$|\psi(t)\rangle = \sum_{N=0}^{3}\sum_{m=0}^{N} C_{m,N-m}|m, N-m\rangle, \tag{28}$$

where C_{mn} are probability amplitudes corresponding to state $|m, n\rangle$. By solving the Schrödinger equation

$$i|\dot{\psi}(t)\rangle = \hat{H}_{e2}|\psi(t)\rangle, \tag{29}$$

we can obtain the above probability amplitudes C_{mn}. When a weak-driving field is applied to the cavity, it may excite a few photons in the cavity. Therefore, we can approximate the probability amplitudes of the excitations as $C_{m,N-m} \sim (\xi/\gamma)^N$. Here, we use the perturbation method [94] to solve the equations of motion for the probability amplitudes

$C_{m,N-m}(t)$. Then, we have the equations of motion for probability amplitudes,

$$\begin{aligned}
i\dot{C}_{00}(t) &= 0,\\
i\dot{C}_{01}(t) &= \Delta_4 C_{01}(t) + JC_{10}(t),\\
i\dot{C}_{10}(t) &= \Delta_3 C_{10}(t) + JC_{01}(t) + \xi C_{00}(t),\\
i\dot{C}_{02}(t) &= 2\Delta_6 C_{02}(t) + \sqrt{2}JC_{11}(t),\\
i\dot{C}_{11}(t) &= (\Delta_5 + \Delta_6)C_{11}(t) + \sqrt{2}JC_{20}(t) + \sqrt{2}JC_{02}(t)\\
&\quad + \xi C_{01}(t),\\
i\dot{C}_{20}(t) &= 2\Delta_5 C_{20}(t) + \sqrt{2}JC_{11}(t) + \sqrt{2}\xi C_{10}(t),\\
i\dot{C}_{03}(t) &= 3\Delta_8 C_{03}(t) + \sqrt{3}JC_{12}(t),\\
i\dot{C}_{12}(t) &= (\Delta_7 + 2\Delta_8)C_{12}(t) + 2JC_{21}(t) + \sqrt{3}JC_{03}(t)\\
&\quad + \xi C_{02}(t),\\
i\dot{C}_{21}(t) &= (2\Delta_7 + \Delta_8)C_{21}(t) + \sqrt{3}JC_{30}(t) + 2JC_{12}(t)\\
&\quad + \sqrt{2}\xi C_{11}(t),\\
i\dot{C}_{30}(t) &= 3\Delta_7 C_{30}(t) + \sqrt{3}JC_{21}(t) + \sqrt{3}\xi C_{20}(t),
\end{aligned} \tag{30}$$

where

$$\begin{aligned}
\Delta_3 &= \Delta_1 - i\gamma/2, \quad \Delta_4 = \Delta_2 - i\gamma/2,\\
\Delta_5 &= \Delta_3 + \chi, \quad \Delta_6 = \Delta_4 + \chi,\\
\Delta_7 &= \Delta_5 + \chi, \quad \Delta_8 = \Delta_6 + \chi.
\end{aligned} \tag{31}$$

By considering the initial condition $C_{00}(0) = 1$ and setting $\dot{C}_{mn}(t) = 0$, we can obtain the steady-state solutions of the probability amplitudes,

$$\begin{aligned}
C_{10} &= \frac{\xi\Delta_4}{\eta_1}, \quad C_{01} = \frac{-\xi J}{\eta_1},\\
C_{02} &= \frac{J^2\xi^2\sigma_1}{\sqrt{2}\eta_1\eta_2\sigma_2}, \quad C_{11} = -\frac{J\xi^2\Delta_6\sigma_1}{\eta_1\eta_2},\\
C_{20} &= \frac{\xi^2\left(\Delta_4\Delta_6/\sigma_2 + J^2\chi\right)}{\sqrt{2}\eta_1\eta_2\sigma_2},\\
C_{03} &= -\frac{J^3\xi^3\Gamma_4}{\sqrt{6}\sigma_2\mu\eta_1\eta_2}, \quad C_{12} = \frac{J^2\xi^3\Delta_8\Gamma_4}{\sqrt{2}\sigma_2\mu\eta_1\eta_2},\\
C_{21} &= \frac{J\xi^3[\Gamma_3 - \Delta_3\eta_3(\Delta_3 + 4\chi)]}{\sqrt{2}\sigma_2\mu\eta_1\eta_2},\\
C_{30} &= \frac{\xi^3(\eta_3\Gamma_1 - \Delta_8\Gamma_2)}{\sqrt{6}\sigma_2\mu\eta_1\eta_2},
\end{aligned} \tag{32}$$

with

$$\begin{aligned}
\sigma_1 &= \Delta_4 + \Delta_5, \quad \sigma_2 = \Delta_5 + \Delta_6,\\
\sigma_3 &= \Delta_7 + \Delta_8, \quad \zeta = \sigma_2^2 + \sigma_3\Delta_7 - 4J^2,\\
\eta_1 &= J^2 - \Delta_3\Delta_4, \quad \eta_2 = J^2 - \Delta_5\Delta_6,\\
\eta_3 &= J^2 - \Delta_7\Delta_8, \quad \mu = \eta_3\left(\eta_3 - 2\sigma_3^2\right),\\
\Gamma_1 &= (\sigma_3 + \Delta_7)(J^2\chi + \sigma_2\Delta_4\Delta_6),\\
\Gamma_2 &= J^2[2\sigma_1(J^2 + 2\sigma_3\Delta_6) - \chi\zeta] + \sigma_2\Delta_4\Delta_6\zeta,\\
\Gamma_3 &= \left(2\Delta_8^2 - \eta_3\right)[J^2\chi + \Delta_6(\sigma_2\Delta_4 + 2\sigma_1\Delta_7)],\\
\Gamma_4 &= \sigma_1(\eta_3 - 4\Delta_6\Delta_7) - 2(J^2\chi + \sigma_2\Delta_4\Delta_6).
\end{aligned} \tag{33}$$

The probabilities of finding m photons in the CW mode and n photons in the CCW mode are given by

$$P_{mn} = \frac{|C_{mn}|^2}{\mathcal{M}}, \tag{34}$$

with the normalization coefficient

$$\mathcal{M} = \sum_{N=0}^{3}\sum_{m=0}^{N}|C_{mn}|^2. \tag{35}$$

The mean photon number is expressed as

$$\begin{aligned}
N &= \langle\hat{a}_1^\dagger\hat{a}_1\rangle \simeq P_{10} + P_{11} + 2P_{20}\\
&= \left|\frac{\xi\Delta_4}{\eta_1}\right|^2 + \left|-\frac{J\xi^2\Delta_6\sigma_1}{\eta_1\eta_2}\right|^2 + 2\left|\frac{\xi^2\left(\Delta_4\Delta_6/\sigma_2 + J^2\chi\right)}{\sqrt{2}\eta_1\eta_2\sigma_2}\right|^2.
\end{aligned} \tag{36}$$

Similarly, for $\Delta_L = 0$, the Sagnac-Fizeau shift and its odd power, which are included in P_{11} and P_{20}, lead to classical nonreciprocity with a resonant drive, as shown in Fig. 2(b).

The second-order correlation function is written as

$$g^{(2)}(0) = \frac{\langle\hat{a}_1^{\dagger 2}\hat{a}_1^2\rangle}{\langle\hat{a}_1^\dagger\hat{a}_1\rangle^2} \simeq \frac{\eta_1^2(\Delta_4\Delta_6/\sigma_2 + J^2\chi)^2}{\eta_2^2\sigma_2^2\Delta_4^4}. \tag{37}$$

The correlation function can be calculated numerically by solving the quantum master equation [95,96]

$$\dot{\hat{\rho}} = i[\hat{\rho}, \hat{H}_2] + \sum_{j=1,2}\frac{\gamma}{2}(2\hat{a}_j\hat{\rho}\hat{a}_j^\dagger - \hat{a}_j^\dagger\hat{a}_j\hat{\rho} - \hat{\rho}\hat{a}_j^\dagger\hat{a}_j). \tag{38}$$

The photon-number probability is $P_{mn} = \langle m, n|\hat{\rho}_{ss}|mn\rangle$, which can be obtained from the steady-state solutions $\hat{\rho}_{ss}$ of the master equation. Excellent agreement between the analytical and numerical results is seen in Figs. 2(c) and 2(d).

Figure 2 shows quantum and classical nonreciprocities with backscattering. In Fig. 2(b), for the resonant cases, we find that the switch between CNR and QNR can still be achieved by tuning the angular velocity Ω after considering the effect of backscattering. When Ω from 0 to 6 kHz, the classical nonreciprocity ($\mathcal{R}_1 \neq 0$) appears, but there is no quantum nonreciprocity ($\mathcal{R}_2 = 0$). Adding Ω beyond 17 kHz, the opposite occurs.

Different from the above resonant cases, Fig. 2(c) shows that no classical nonreciprocity occurs at $\Delta_L = -0.98$ kHz by fixing the rotational speed to $\Omega = 3.8$ kHz. In addition, for $J/\gamma = 2$, the number of peaks of N increased from one to two, compared with an ideal resonator (Fig. 1). A similar feature can also be identified in the number of dips of $g^{(2)}(0)$ in Fig. 2(d). The reason is that the energy-level splitting caused by backscattering provides the possibility of more photon jumps. This means we can explore the richer significance of nonreciprocity by combining backscattering and mechanical rotation.

As shown in Fig. 3(a), for $J/\gamma < 0.7$, the second-order correlation functions of the two modes are reciprocal

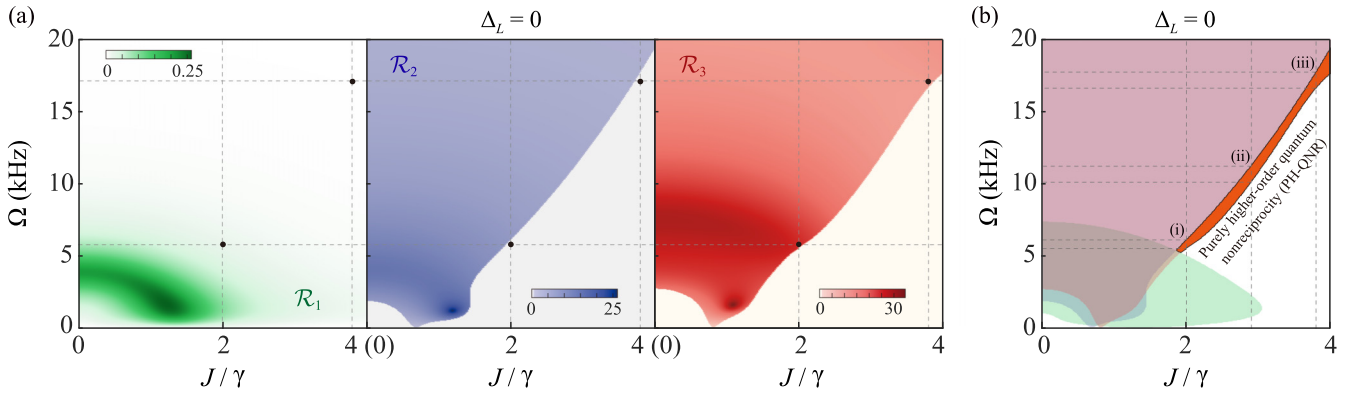

FIG. 3. (a) The classical nonreciprocity ratio $\mathcal{R}_1$, the quantum nonreciprocity ratio $\mathcal{R}_2$, and the higher-order quantum nonreciprocity ratio $\mathcal{R}_3$ obtained as a function of backscattering rate J and angular velocity Ω. (b) The purely higher-order quantum nonreciprocity (PH-QNR) versus J and Ω. The other parameters are the same as those in Fig. 1.

($\mathcal{R}_2 = 0$) for smaller angular velocity $\Omega < 1.9$ kHz, which occurs because the mode splitting due to backscattering and the Sagnac-Fizeau shift due to rotation are both small. When $J/\gamma > 0.7$, the minimum angular velocity required for the emergence of quantum nonreciprocity ($\mathcal{R}_2 \neq 0$) increases with increasing backscattering rate. Also, we find that various kinds of nonreciprocity can be switched by tuning the backscattering and mechanical rotation of the resonator for resonant cases (Fig. 3). Further, we extend our research to the higher-order quantum nonreciprocity of this system. The third-order correlation function can be obtained analytically as

$$g^{(3)}(0) = \frac{\langle \hat{a}_1^{\dagger 3} \hat{a}_1^3 \rangle}{\langle \hat{a}_1^{\dagger} \hat{a}_1 \rangle^3} \simeq \frac{\eta_1^4 (\eta_3 \Gamma_1 - \Delta_8 \Gamma_2)^2}{\mu^2 \eta_2^2 \sigma_2^2 \Delta_4^6}. \tag{39}$$

The condition $g^{(3)}(0) < 1$ [$g^{(3)}(0) > 1$] indicates third-order sub-Poissonian (super-Poissonian) statistics, which was also interpreted as three-photon antibunching (bunching) in recent experiments on multiphoton blockade [101] and photon-induced tunneling [102]. Like in Eq. (8), we define a higher-order quantum nonreciprocity ratio $\mathcal{R}_3$, which is written as

$$\mathcal{R}_3 = 10 \log_{10} \frac{g^{(3)}_{\mathrm{CCW}}(0)}{g^{(3)}_{\mathrm{CW}}(0)}. \tag{40}$$

We set $\mathcal{R}_3 = 0$ for the cases in which both $g^{(3)}_{\mathrm{CCW}}(0)$ and $g^{(3)}_{\mathrm{CW}}(0)$ are smaller or larger than 1. The difference is that the condition of PH-QNR needs to satisfy not only $\mathcal{R}_3 \neq 0$ but also the condition of reciprocity of the classical mean photon number ($\mathcal{R}_1 = 0$) and quantum second-order correlation function ($\mathcal{R}_2 = 0$).

Figure 3(b) shows the relationship of PH-QNR with backscattering and angular velocity for the resonant cases. We find that PH-QNR occurs as the backscattering rate J increases beyond a certain point. For $J/\gamma = 2$ [Fig. 3(b), (i)], PH-QNR emerges with angular velocity $5.56 \leqslant \Omega \leqslant 6.17$ kHz. This result is in agreement with the results in Figs. 4(a) and 4(b). Increasing J/γ to 2.9, the range of angular velocity Ω corresponding to the appearance of PH-QNR is 10.13–11.28 kHz [Fig. 3(b), (ii)]. By further increasing the backscattering rate ($J/\gamma = 3.8$), the corresponding Ω is increased to 16.59–17.74 kHz [Fig. 3(b), (iii)]. This shows that the minimum angular velocity Ω required for the emergence of PH-QNR increases with increasing backscattering rate J. We also find that PH-QNR can be achieved by controlling the angular velocity and the backscattering rate of the resonator for the resonant cases [Fig. 3(b)].

Figures 4(a) and 4(b) show that PH-QNR occurs around $\Delta_L = -0.67$ kHz. At this point, for different input directions, the third-order correlation functions are nonreciprocal [$g^{(3)}_{\mathrm{CW}}(0) \sim 0.86$, $g^{(3)}_{\mathrm{CCW}}(0) \sim 272.68$], but the second-order correlation functions and the mean photon numbers are reciprocal, i.e., $g^{(2)}_{\mathrm{CW}}(0) > 1$, $g^{(2)}_{\mathrm{CCW}}(0) > 1$, and $N_{\mathrm{CW}} = N_{\mathrm{CCW}}$. As far as we know, this purely higher-order quantum nonreciprocity was not revealed in previous works on the nonreciprocal effect.

To clearly show the difference in nonreciprocities between the ideal cavity ($J = 0$) and the realistic cavity ($J/\gamma = 2$), we compare the nonreciprocity ratios of the above different cases, as shown in Figs. 4(c)–4(h). We find that backscattering has a small effect on the classical nonreciprocity [see Figs. 4(c) and 4(f)] but a large effect on the quantum nonreciprocity; for example, the negative value of $\mathcal{R}_3$ appears in Fig. 4(h). By comparison, we note that the purely higher-order quantum nonreciprocity occurs in the realistic cavity due to the effect of backscattering but not in an ideal cavity.

V. CONCLUSIONS

In summary, we studied the coherent switch of classical and quantum nonreciprocities of photons and realized purely higher-order quantum nonreciprocity by using a spinning Kerr resonator. Our findings contain three main features. First, we showed a single device switching between a classical isolator and a purely quantum directional system by adjusting multiple degrees of freedom (the optical detuning Δ_L and angular velocity Ω). Furthermore, we presented the purely higher-order quantum nonreciprocity, which provides a richer degree of freedom for one-way optical control; that is, it is able to achieve one-way quantum communication while classical communication is reciprocal. More interestingly, in practical devices, backscattering is unavoidable, but it can induce purely higher-order quantum nonreciprocity. These

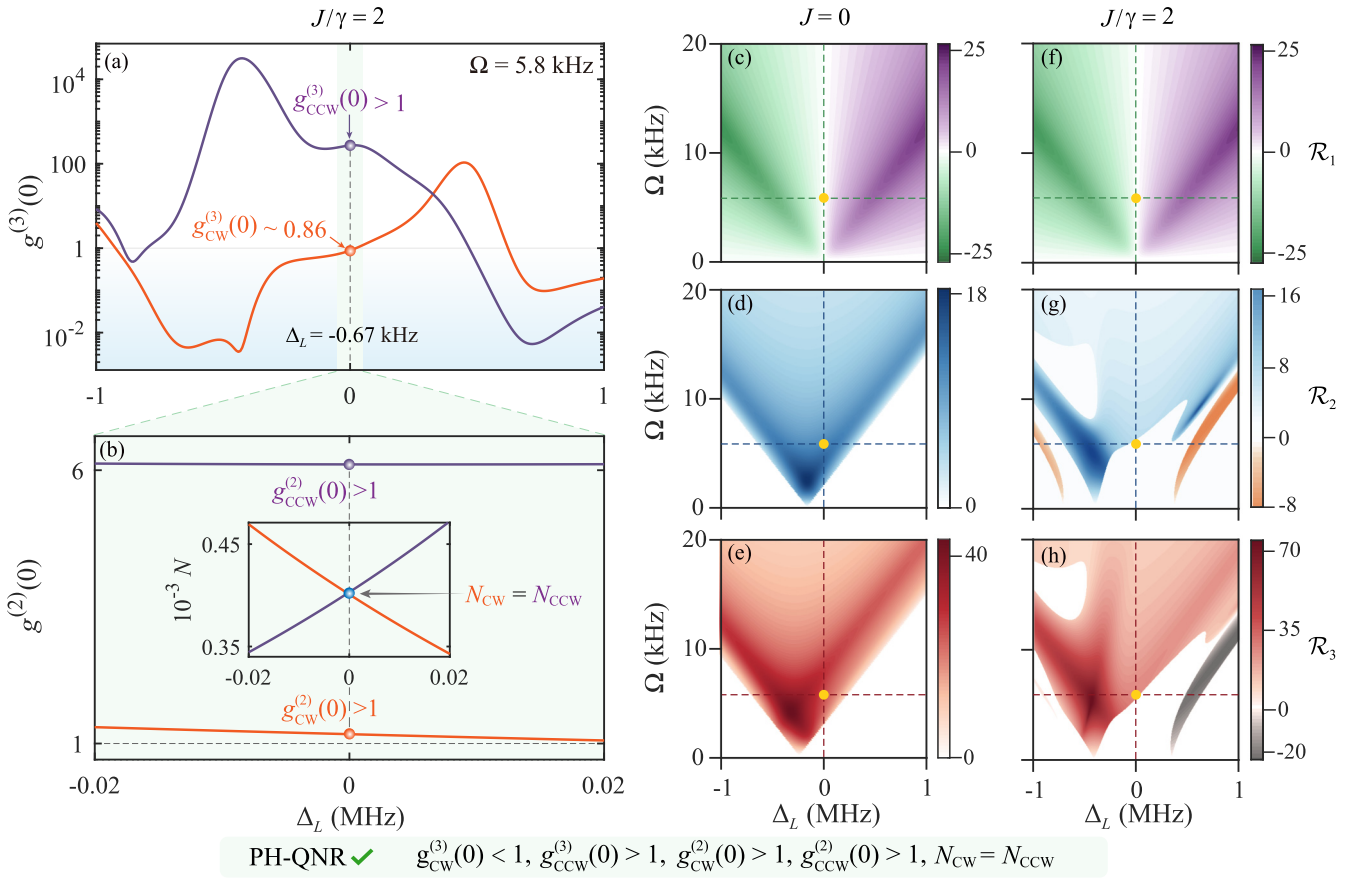

FIG. 4. The backscattering-induced PH-QNR. (a) and (b) The correlation functions $g^{(3)}(0)$ and $g^{(2)}(0)$ and the mean photon number N versus the optical detuning Δ_L for $J/\gamma = 2$ and $\Omega = 5.8$ kHz (i.e., $\Omega/\gamma = 0.024$). (c)–(h) For the generation of PH-QNR, the comparison between the cases with and without backscattering. The other parameters are the same as those in Fig. 1.

results offer the possibility of new developments in nonreciprocal devices and have potential applications in nanoparticle sensing. We believe that our work can be extended to spinning photonics and spinning optomechanics with similar backscattering.

ACKNOWLEDGMENTS

H.J. is supported by the National Natural Science Foundation of China (Grants No. 11935006 and No. 11774086) and the Science and Technology Innovation Program of Hunan Province (Grant No. 2020RC4047). R.H. is supported by the Japan Society for the Promotion of Science (JSPS) Postdoctoral Fellowships for Research in Japan (No. P22018). X.-W.X. is supported by the National Natural Science Foundation of China (Grants No. 12064010 and No. 12247105), the Natural Science Foundation of Hunan Province of China (Grant No. 2021JJ20036), and the Science and Technology Innovation Program of Hunan Province (Grant No. 2022RC1203).

[1] Y. Shoji and T. Mizumoto, Magneto-optical non-reciprocal devices in silicon photonics, Sci. Technol. Adv. Mater. **15**, 014602 (2014).

[2] J. D. Adam, L. E. Davis, G. F. Dionne, E. F. Schloemann, and S. N. Stitzer, Ferrite devices and materials, IEEE Trans. Microwave Theory Tech. **50**, 721 (2002).

[3] H. Dötsch, N. Bahlmann, O. Zhuromskyy, M. Hammer, L. Wilkens, R. Gerhardt, P. Hertel, and A. F. Popkov, Applications of magneto-optical waveguides in integrated optics: Review, J. Opt. Soc. Am. B **22**, 240 (2005).

[4] Z. Yu and S. Fan, Complete optical isolation created by indirect interband photonic transitions, Nat. Photonics **3**, 91 (2009).

[5] M. S. Kang, A. Butsch, and P. St. J. Russell, Reconfigurable light-driven opto-acoustic isolators in photonic crystal fibre, Nat. Photonics **5**, 549 (2011).

[6] N. A. Estep, D. L. Sounas, J. Soric, and A. Alù, Magnetic-free non-reciprocity and isolation based on parametrically modulated coupled-resonator loops, Nat. Phys. **10**, 923 (2014).

[7] L. D. Tzuang, K. Fang, P. Nussenzveig, S. Fan, and M. Lipson, Non-reciprocal phase shift induced by an effective magnetic flux for light, Nat. Photonics **8**, 701 (2014).

[8] T. T. Koutserimpas and R. Fleury, Nonreciprocal gain in non-Hermitian time-Floquet systems, Phys. Rev. Lett. **120**, 087401 (2018).

[9] E. A. Kittlaus, N. T. Otterstrom, P. Kharel, S. Gertler, and P. T. Rakich, Non-reciprocal interband Brillouin modulation, Nat. Photonics **12**, 613 (2018).

[10] X. Guo, Y. Ding, Y. Duan, and X. Ni, Nonreciprocal metasurface with space–time phase modulation, Light: Sci. Appl. **8**, 123 (2019).

[11] X. Wang, G. Ptitcyn, V. S. Asadchy, A. Díaz-Rubio, M. S. Mirmoosa, S. Fan, and S. A. Tretyakov, Nonreciprocity in bianisotropic systems with uniform time modulation, Phys. Rev. Lett. **125**, 266102 (2020).

[12] L. Fan, J. Wang, L. T. Varghese, H. Shen, B. Niu, Y. Xuan, A. M. Weiner, and M. Qi, An all-silicon passive optical diode, Science **335**, 447 (2012).

[13] H. Z. Shen, Y. H. Zhou, and X. X. Yi, Quantum optical diode with semiconductor microcavities, Phys. Rev. A **90**, 023849 (2014).

[14] Q.-T. Cao, H. Wang, C.-H. Dong, H. Jing, R.-S. Liu, X. Chen, L. Ge, Q. Gong, and Y.-F. Xiao, Experimental demonstration of spontaneous chirality in a nonlinear microresonator, Phys. Rev. Lett. **118**, 033901 (2017).

[15] X.-W. Xu, Y. Li, B. Li, H. Jing, and A.-X. Chen, Nonreciprocity via nonlinearity and synthetic magnetism, Phys. Rev. Appl. **13**, 044070 (2020).

[16] Q.-T. Cao, R. Liu, H. Wang, Y.-K. Lu, C.-W. Qiu, S. Rotter, Q. Gong, and Y.-F. Xiao, Reconfigurable symmetry-broken laser in a symmetric microcavity, Nat. Commun. **11**, 1136 (2020).

[17] S. Manipatruni, J. T. Robinson, and M. Lipson, Optical nonreciprocity in optomechanical structures, Phys. Rev. Lett. **102**, 213903 (2009).

[18] C.-H. Dong, Z. Shen, C.-L. Zou, Y.-L. Zhang, W. Fu, and G.-C. Guo, Brillouin-scattering-induced transparency and non-reciprocal light storage, Nat. Commun. **6**, 6193 (2015).

[19] J. Kim, M. C. Kuzyk, K. Han, H. Wang, and G. Bahl, Non-reciprocal Brillouin scattering induced transparency, Nat. Phys. **11**, 275 (2015).

[20] Z. Shen, Y.-L. Zhang, Y. Chen, C.-L. Zou, Y.-F. Xiao, X.-B. Zou, F.-W. Sun, G.-C. Guo, and C.-H. Dong, Experimental realization of optomechanically induced non-reciprocity, Nat. Photonics **10**, 657 (2016).

[21] F. Ruesink, M.-A. Miri, A. Alù, and E. Verhagen, Nonreciprocity and magnetic-free isolation based on optomechanical interactions, Nat. Commun. **7**, 13662 (2016).

[22] S. Hua, J. Wen, X. Jiang, Q. Hua, L. Jiang, and M. Xiao, Demonstration of a chip-based optical isolator with parametric amplification, Nat. Commun. **7**, 13657 (2016).

[23] N. R. Bernier, L. D. Tóth, A. Koottandavida, M. A. Ioannou, D. Malz, A. Nunnenkamp, A. K. Feofanov, and T. J. Kippenberg, Nonreciprocal reconfigurable microwave optomechanical circuit, Nat. Commun. **8**, 604 (2017).

[24] M.-A. Miri, F. Ruesink, E. Verhagen, and A. Alù, Optical nonreciprocity based on optomechanical coupling, Phys. Rev. Appl. **7**, 064014 (2017).

[25] Z. Shen, Y.-L. Zhang, Y. Chen, F.-W. Sun, X.-B. Zou, G.-C. Guo, C.-L. Zou, and C.-H. Dong, Reconfigurable optomechanical circulator and directional amplifier, Nat. Commun. **9**, 1797 (2018).

[26] A. Rosario Hamann, C. Müller, M. Jerger, M. Zanner, J. Combes, M. Pletyukhov, M. Weides, T. M. Stace, and A. Fedorov, Nonreciprocity realized with quantum nonlinearity, Phys. Rev. Lett. **121**, 123601 (2018).

[27] D. L. Sounas and A. Alù, Nonreciprocity based on nonlinear resonances, IEEE Antennas Wireless Propag. Lett. **17**, 1958 (2018).

[28] L. Mercier de Lépinay, E. Damskägg, C. F. Ockeloen-Korppi, and M. A. Sillanpää, Realization of directional amplification in a microwave optomechanical device, Phys. Rev. Appl. **11**, 034027 (2019).

[29] X. Xu, Y. Zhao, H. Wang, H. Jing, and A. Chen, Quantum nonreciprocality in quadratic optomechanics, Photonics Res. **8**, 143 (2020).

[30] L. Tang, J. Tang, H. Wu, J. Zhang, M. Xiao, and K. Xia, Broad-intensity-range optical nonreciprocity based on feedback-induced Kerr nonlinearity, Photonics Res. **9**, 1218 (2021).

[31] Z. Shen, Y.-L. Zhang, Y. Chen, Y.-F. Xiao, C.-L. Zou, G.-C. Guo, and C.-H. Dong, Nonreciprocal frequency conversion and mode routing in a microresonator, Phys. Rev. Lett. **130**, 013601 (2023).

[32] H. Ramezani, T. Kottos, R. El-Ganainy, and D. N. Christodoulides, Unidirectional nonlinear $\mathcal{PT}$-symmetric optical structures, Phys. Rev. A **82**, 043803 (2010).

[33] B. Peng, Ş. K. Özdemir, F. Lei, F. Monifi, M. Gianfreda, G. L. Long, S. Fan, F. Nori, C. M. Bender, and L. Yang, Parity–time-symmetric whispering-gallery microcavities, Nat. Phys. **10**, 394 (2014).

[34] L. Chang, X. Jiang, S. Hua, C. Yang, J. Wen, L. Jiang, G. Li, G. Wang, and M. Xiao, Parity– time symmetry and variable optical isolation in active– passive-coupled microresonators, Nat. Photonics **8**, 524 (2014).

[35] X. Huang, C. Lu, C. Liang, H. Tao, and Y.-C. Liu, Loss-induced nonreciprocity, Light: Sci. Appl. **10**, 30 (2021).

[36] L. Tang, J. Tang, M. Chen, F. Nori, M. Xiao, and K. Xia, Quantum squeezing induced optical nonreciprocity, Phys. Rev. Lett. **128**, 083604 (2022).

[37] D.-W. Wang, H.-T. Zhou, M.-J. Guo, J.-X. Zhang, J. Evers, and S.-Y. Zhu, Optical diode made from a moving photonic crystal, Phys. Rev. Lett. **110**, 093901 (2013).

[38] K. Xia, F. Nori, and M. Xiao, Cavity-free optical isolators and circulators using a chiral cross-Kerr nonlinearity, Phys. Rev. Lett. **121**, 203602 (2018).

[39] S. Zhang, Y. Hu, G. Lin, Y. Niu, K. Xia, J. Gong, and S. Gong, Thermal-motion-induced non-reciprocal quantum optical system, Nat. Photonics **12**, 744 (2018).

[40] C. Liang, B. Liu, A.-N. Xu, X. Wen, C. Lu, K. Xia, M. K. Tey, Y.-C. Liu, and L. You, Collision-induced broadband optical nonreciprocity, Phys. Rev. Lett. **125**, 123901 (2020).

[41] M.-X. Dong, K.-Y. Xia, W.-H. Zhang, Y.-C. Yu, Y.-H. Ye, E.-Z. Li, L. Zeng, D.-S. Ding, B.-S. Shi, G.-C. Guo, and F. Nori, All-optical reversible single-photon isolation at room temperature, Sci. Adv. **7**, eabe8924 (2021).

[42] F. Song, Z. Wang, E. Li, B. Yu, and Z. Huang, Nonreciprocity with structured light using optical pumping in hot atoms, Phys. Rev. Appl. **18**, 024027 (2022).

[43] H. Lü, Y. Jiang, Y.-Z. Wang, and H. Jing, Optomechanically induced transparency in a spinning resonator, Photonics Res. **5**, 367 (2017).

[44] S. Maayani, R. Dahan, Y. Kligerman, E. Moses, A. U. Hassan, H. Jing, F. Nori, D. N. Christodoulides, and T. Carmon,

Flying couplers above spinning resonators generate irreversible refraction, Nature (London) **558**, 569 (2018).
[45] Y. Jiang, S. Maayani, T. Carmon, F. Nori, and H. Jing, Nonreciprocal phonon laser, Phys. Rev. Appl. **10**, 064037 (2018).
[46] R. Huang, A. Miranowicz, J.-Q. Liao, F. Nori, and H. Jing, Nonreciprocal photon blockade, Phys. Rev. Lett. **121**, 153601 (2018).
[47] B. Li, R. Huang, X. Xu, A. Miranowicz, and H. Jing, Nonreciprocal unconventional photon blockade in a spinning optomechanical system, Photonics Res. **7**, 630 (2019).
[48] K. Wang, Q. Wu, Y.-F. Yu, and Z.-M. Zhang, Nonreciprocal photon blockade in a two-mode cavity with a second-order nonlinearity, Phys. Rev. A **100**, 053832 (2019).
[49] H. Z. Shen, Q. Wang, J. Wang, and X. X. Yi, Nonreciprocal unconventional photon blockade in a driven dissipative cavity with parametric amplification, Phys. Rev. A **101**, 013826 (2020).
[50] Y.-W. Jing, H.-Q. Shi, and X.-W. Xu, Nonreciprocal photon blockade and directional amplification in a spinning resonator coupled to a two-level atom, Phys. Rev. A **104**, 033707 (2021).
[51] Y.-F. Jiao, S.-D. Zhang, Y.-L. Zhang, A. Miranowicz, L.-M. Kuang, and H. Jing, Nonreciprocal optomechanical entanglement against backscattering losses, Phys. Rev. Lett. **125**, 143605 (2020).
[52] Z.-B. Yang, J.-S. Liu, A.-D. Zhu, H.-Y. Liu, and R.-C. Yang, Nonreciprocal transmission and nonreciprocal entanglement in a spinning microwave magnomechanical system, Ann. Phys. (Berlin, Ger.) **532**, 2000196 (2020).
[53] Y.-L. Ren, Nonreciprocal optical– microwave entanglement in a spinning magnetic resonator, Opt. Lett. **47**, 1125 (2022).
[54] Y.-F. Jiao, J.-X. Liu, Y. Li, R. Yang, L.-M. Kuang, and H. Jing, Nonreciprocal enhancement of remote entanglement between nonidentical mechanical oscillators, Phys. Rev. Appl. **18**, 064008 (2022).
[55] I. M. Mirza, W. Ge, and H. Jing, Optical nonreciprocity and slow light in coupled spinning optomechanical resonators, Opt. Express **27**, 25515 (2019).
[56] W.-A. Li, G.-Y. Huang, J.-P. Chen, and Y. Chen, Nonreciprocal enhancement of optomechanical second-order sidebands in a spinning resonator, Phys. Rev. A **102**, 033526 (2020).
[57] D.-W. Zhang, L.-L. Zheng, C. You, C.-S. Hu, Y. Wu, and X.-Y. Lü, Nonreciprocal chaos in a spinning optomechanical resonator, Phys. Rev. A **104**, 033522 (2021).
[58] B. Li, Ş. K. Özdemir, X.-W. Xu, L. Zhang, L.-M. Kuang, and H. Jing, Nonreciprocal optical solitons in a spinning Kerr resonator, Phys. Rev. A **103**, 053522 (2021).
[59] Y. Xu, J.-Y. Liu, W. Liu, and Y.-F. Xiao, Nonreciprocal phonon laser in a spinning microwave magnomechanical system, Phys. Rev. A **103**, 053501 (2021).
[60] X. Shang, H. Xie, G. Lin, and X. Lin, Nonreciprocity steered with a spinning resonator, Photonics **9**, 585 (2022).
[61] Z. Yang, Y. Cheng, N. Wang, Y. Chen, and S. Wang, Nonreciprocal light propagation induced by a subwavelength spinning cylinder, Opt. Express **30**, 27993 (2022).
[62] R. Fleury, D. L. Sounas, C. F. Sieck, M. R. Haberman, and A. Alù, Sound isolation and giant linear nonreciprocity in a compact acoustic circulator, Science **343**, 516 (2014).
[63] A. B. Khanikaev, R. Fleury, S. H. Mousavi, and A. Alù, Topologically robust sound propagation in an angular-momentum-biased graphene-like resonator lattice, Nat. Commun. **6**, 8260 (2015).
[64] X. Xu, Q. Wu, H. Chen, H. Nassar, Y. Chen, A. Norris, M. R. Haberman, and G. Huang, Physical observation of a robust acoustic pumping in waveguides with dynamic boundary, Phys. Rev. Lett. **125**, 253901 (2020).
[65] H. Jing, H. Lü, S. K. Özdemir, T. Carmon, and F. Nori, Nanoparticle sensing with a spinning resonator, Optica **5**, 1424 (2018).
[66] J. Ahn, Z. Xu, J. Bang, P. Ju, X. Gao, and T. Li, Ultrasensitive torque detection with an optically levitated nanorotor, Nat. Nanotechnol. **15**, 89 (2020).
[67] H. Zhang, R. Huang, S.-D. Zhang, Y. Li, C.-W. Qiu, F. Nori, and H. Jing, Breaking anti-PT symmetry by spinning a resonator, Nano Lett. **20**, 7594 (2020).
[68] X. Mao, H. Yang, D. Long, M. Wang, P.-Y. Wen, Y.-Q. Hu, B.-Y. Wang, G.-Q. Li, J.-C. Gao, and G.-L. Long, Experimental demonstration of mode-matching and Sagnac effect in a millimeter-scale wedged resonator gyroscope, Photonics Res. **10**, 2115 (2022).
[69] I. H. Grinberg, M. Lin, C. Harris, W. A. Benalcazar, C. W. Peterson, T. L. Hughes, and G. Bahl, Robust temporal pumping in a magneto-mechanical topological insulator, Nat. Commun. **11**, 974 (2020).
[70] G. Xu, K. Dong, Y. Li, H. Li, K. Liu, L. Li, J. Wu, and C.-W. Qiu, Tunable analog thermal material, Nat. Commun. **11**, 6028 (2020).
[71] L. Dong and Y. V. Kartashov, Rotating multidimensional quantum droplets, Phys. Rev. Lett. **126**, 244101 (2021).
[72] Z. Zhu, X. Ren, W. Sha, M. Xiao, R. Hu, and X. Luo, Inverse design of rotating metadevice for adaptive thermal cloaking, Int. J. Heat Mass Transfer **176**, 121417 (2021).
[73] L. Xu, J. Liu, P. Jin, G. Xu, J. Li, X. Ouyang, Y. Li, C.-W. Qiu, and J. Huang, Black-hole-inspired thermal trapping with graded heat-conduction metadevices, Natl. Sci. Rev. **10**, nwac159 (2023).
[74] P. Yang, M. Li, X. Han, H. He, G. Li, C.-L. Zou, P. Zhang, Y. Qian, and T. Zhang, Non-reciprocal cavity polariton with atoms strongly coupled to optical cavity, Laser Photonics Rev. **17**, 2200574 (2023).
[75] A. Graf, S. D. Rogers, J. Staffa, U. A. Javid, D. H. Griffith, and Q. Lin, Nonreciprocity in photon pair correlations of classically reciprocal systems, Phys. Rev. Lett. **128**, 213605 (2022).
[76] C. Gonzalez-Ballestero, A. Gonzalez-Tudela, F. J. Garcia-Vidal, and E. Moreno, Chiral route to spontaneous entanglement generation, Phys. Rev. B **92**, 155304 (2015).
[77] H. J. Kimble, The quantum internet, Nature (London) **453**, 1023 (2008).
[78] P. Lodahl, S. Mahmoodian, S. Stobbe, A. Rauschenbeutel, P. Schneeweiss, J. Volz, H. Pichler, and P. Zoller, Chiral quantum optics, Nature (London) **541**, 473 (2017).
[79] S. A. H. Gangaraj, G. W. Hanson, and M. Antezza, Robust entanglement with three-dimensional nonreciprocal photonic topological insulators, Phys. Rev. A **95**, 063807 (2017).
[80] R. Fleury, D. Sounas, and A. Alù, An invisible acoustic sensor based on parity-time symmetry, Nat. Commun. **6**, 5905 (2015).

[81] T. Yang, X. Bai, D. Gao, L. Wu, B. Li, J. T. L. Thong, and C.-W. Qiu, Invisible sensors: Simultaneous sensing and camouflaging in multiphysical fields, Adv. Mater. **27**, 7752 (2015).
[82] I. Schuster, A. Kubanek, A. Fuhrmanek, T. Puppe, P. W. H. Pinkse, K. Murr, and G. Rempe, Nonlinear spectroscopy of photons bound to one atom, Nat. Phys. **4**, 382 (2008).
[83] G. B. Malykin, The Sagnac effect: Correct and incorrect explanations, Phys. Usp. **43**, 1229 (2000).
[84] K. J. Vahala, Optical microcavities, Nature (London) **424**, 839 (2003).
[85] S. M. Spillane, T. J. Kippenberg, K. J. Vahala, K. W. Goh, E. Wilcut, and H. J. Kimble, Ultrahigh-Q toroidal microresonators for cavity quantum electrodynamics, Phys. Rev. A **71**, 013817 (2005).
[86] N. G. Pavlov, G. Lihachev, S. Koptyaev, E. Lucas, M. Karpov, N. M. Kondratiev, I. A. Bilenko, T. J. Kippenberg, and M. L. Gorodetsky, Soliton dual frequency combs in crystalline microresonators, Opt. Lett. **42**, 514 (2017).
[87] V. Huet, A. Rasoloniaina, P. Guillemé, P. Rochard, P. Féron, M. Mortier, A. Levenson, K. Bencheikh, A. Yacomotti, and Y. Dumeige, Millisecond photon lifetime in a slow-light microcavity, Phys. Rev. Lett. **116**, 133902 (2016).
[88] J. A. Zielińska and M. W. Mitchell, Self-tuning optical resonator, Opt. Lett. **42**, 5298 (2017).
[89] A. Faraon, I. Fushman, D. Englund, N. Stoltz, P. Petroff, and J. Vučković, Coherent generation of non-classical light on a chip via photon-induced tunnelling and blockade, Nat. Phys. **4**, 859 (2008).
[90] A. Majumdar, M. Bajcsy, A. Rundquist, and J. Vučković, Loss-enabled sub-poissonian light generation in a bimodal nanocavity, Phys. Rev. Lett. **108**, 183601 (2012).
[91] M. O. Scully and M. S. Zubairy, *Quantum Optics* (Cambridge University Press, Cambridge, 1997).
[92] A. Miranowicz, M. Bartkowiak, X. Wang, Y.-X. Liu, and F. Nori, Testing nonclassicality in multimode fields: A unified derivation of classical inequalities, Phys. Rev. A **82**, 013824 (2010).
[93] M. B. Plenio and P. L. Knight, The quantum-jump approach to dissipative dynamics in quantum optics, Rev. Mod. Phys. **70**, 101 (1998).
[94] H. J. Carmichael, R. J. Brecha, and P. R. Rice, Quantum interference and collapse of the wavefunction in cavity QED, Opt. Commun. **82**, 73 (1991).
[95] J. R. Johansson, P. D. Nation, and F. Nori, QuTiP: An open-source python framework for the dynamics of open quantum systems, Comput. Phys. Commun. **183**, 1760 (2012).
[96] J. R. Johansson, P. D. Nation, and F. Nori, QuTiP 2: A python framework for the dynamics of open quantum systems, Comput. Phys. Commun. **184**, 1234 (2013).
[97] J. Zhu, S. K. Ozdemir, Y.-F. Xiao, L. Li, L. He, D.-R. Chen, and L. Yang, On-chip single nanoparticle detection and sizing by mode splitting in an ultrahigh-Q microresonator, Nat. Phys. **4**, 46 (2010).
[98] S. Kim, J. M. Taylor, and G. Bahl, Dynamic suppression of Rayleigh backscattering in dielectric resonators, Optica **6**, 1016 (2019).
[99] Z. R. Gong, H. Ian, Y.-X. Liu, C. P. Sun, and F. Nori, Effective Hamiltonian approach to the Kerr nonlinearity in an optomechanical system, Phys. Rev. A **80**, 065801 (2009).
[100] T. T. Heikkilä, F. Massel, J. Tuorila, R. Khan, and M. A. Sillanpää, Enhancing optomechanical coupling via the Josephson effect, Phys. Rev. Lett. **112**, 203603 (2014).
[101] C. Hamsen, K. N. Tolazzi, T. Wilk, and G. Rempe, Two-photon blockade in an atom-driven cavity QED system, Phys. Rev. Lett. **118**, 133604 (2017).
[102] A. Rundquist, M. Bajcsy, A. Majumdar, T. Sarmiento, K. Fischer, K. G. Lagoudakis, S. Buckley, A. Y. Piggott, and J. Vučković, Nonclassical higher-order photon correlations with a quantum dot strongly coupled to a photonic-crystal nanocavity, Phys. Rev. A **90**, 023846 (2014).